RSC Advances

ROYAL SOCIETY OF CHEMISTRY

www.rsc.org/advances

Table of contents entry

Glucose sensing by using of glucose oxidase and a biocompatible poly(p-phenylenediamine)-based nanocomposite

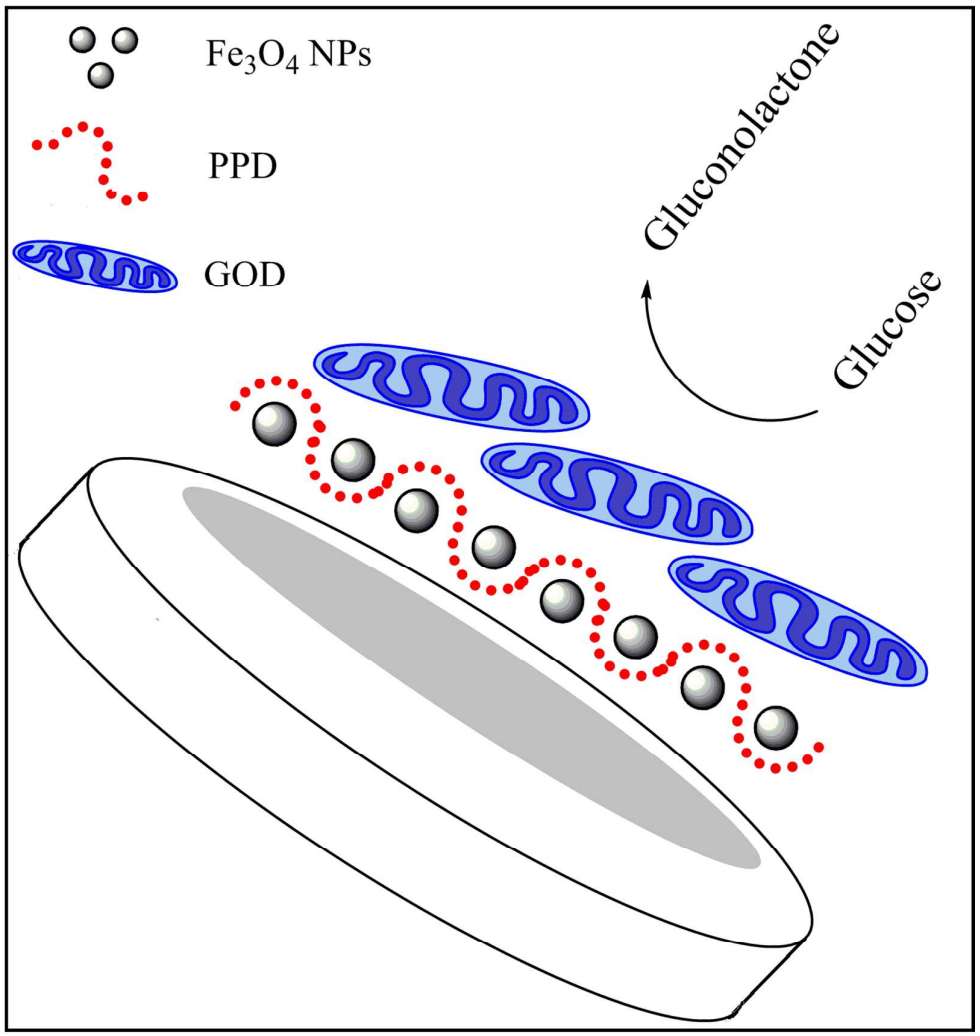

Glucose sensing by a glassy carbon electrode modified with glucose oxidase and a poly(p-phenylenediamine)-based nanocomposite

Mehdi Baghayeri*

Department of Chemistry, Faculty of Science, Hakim Sabzevari University, PO. Box 397, Sabzevar, Iran

*Corresponding author. Tel: +98 5714003325; fax: +98 5714003170

E-mail address: m.baghayeri@hsu.ac.ir

Abstract

In this paper a synthetic nanocomposite based on poly(p-phenylenediamine) (PPD) and Fe_3O_4 nanoparticles (Fe_3O_4 NPs) introduced as a suitable substrate for enzyme immobilization. Glucose oxidase (GOD) was immobilized on PPD@Fe_3O_4 modified glassy carbon electrode (GCE). The immobilized GOD on PPD@Fe_3O_4 nanocomposite displayed a pair of well-defined quasi-reversible redox peaks with a formal potential of -0.41 V (vs. SCE) and a heterogeneous electron transfer rate constant (k_s) of 3.76 s^{-1} in 0.1 M pH 7.0 PBS solution. The apparent Michaelis–Menten constant of the immobilized GOD was 0.42 mM, indicating an excellent catalytic activity and a notable affinity to detection of glucose. There was no interference from compounds commonly found in clinical samples and determination of glucose in clinical samples was successfully presented.

Keywords: Biosensor; Fe_3O_4 nanoparticles; Enzyme immobilization; Glucose oxidase

1. Introduction

High blood glucose has become an important public health problem owing to its growing prevalence and its association with adverse pregnancy outcomes and type 2 diabetes mellitus later in life. The easier, cheaper, reproducible, sensitive and cost-effectiveness glucose tests are acceptable by the World Health Organization (WHO) and the American Diabetes Association (ADA) [1,2]. On this basis, many studies have done to detect glucose in the body biological fluids [3-7]. Among them, glucose biosensors based on the direct electrochemistry of glucose oxidase (GOD) have been attracted extensively over the past years. These glucose biosensors use no expensive or harmful mediators and show the advantages of excellent selectivity and high sensitivity [8-10].

The two bound redox-active flavin adenine dinucleotide (FAD) cofactors of GOD play a central role for direct electron transfer (DET) at glucose biosensor [11]. However, these cofactors are deeply covered up within the isolated prosthetic shells, rendering them inaccessible for DET with bare electrodes [12]. However, many efforts have been taken due to the increase the electron transfer between FAD and electrode surfaces. The using of various nanomaterials such as gold NPs [13], silver NPs [14], carbon nanotubes [15], conductive polymers [16], non-conducting polymers [10], graphene [17] and their composites [18,19] are some of these attempts to improve the performance of glucose biosensors.

Nanocomposites have fascinated more and more attention because of their biocompatibility, biodegradability to harmless products, nontoxicity and physiological inertness [20]. Among various kinds of nanocomposites, polymer-based nanocomposites as very applicable platforms are the most favorable materials that use to promote the electron transfer of redox enzymes, since the unique electronic and structure properties of polymer-based nanocomposites allow good communication between nanocomposites and redox center of enzymes. Xiao et al. developed an amperometric biosensor based on direct

electrochemistry of GOD immobilized on poly(methylene blue) doped silica nanocomposites [21]. Xu et al. reported graphene/polyaniline/gold NPs nanocomposite for the direct electron transfer of GOD [12]. Senel et al. fabricated a glucose biosensor based on immobilization of GOD on poly(pyrrole propylic acid)/Au nanocomposite and the prepared electrode exhibited excellent electrocatalytic activities towards the glucose sensing [22]. On the other hand, multicomponent backbone of these nanocomposites that contain two or more nanometer-scale components can cause to permanent interactions between nanocomposites and enzymes to form the more stable biosensors [23]. We have recently studied the preparation of polymer-based nanocomposites and their applications as amperometric biosensors [23-25].

In this work, GCE was successfully modified using poly(p-phenylenediamine) and Fe_3O_4 NPs (PPD@Fe_3O_4). The functional -NH- groups at PPD paved the way for the Fe_3O_4 loading. The PPD@Fe_3O_4 nanocomposite homogeneously decorated on GCE to fabricate PPD@Fe_3O_4/GCE. Because of the electrical, mechanical and catalytic abilities of both PPD and Fe_3O_4 NPs, the resultant nanocomposite can offer a favorable microenvironment for facilitating DET between enzyme and the electrode surface. Therefore, GOD was simply coated on the PPD@Fe_3O_4/GCE surface by the drop-casting method to fabricate GOD-PPD@Fe_3O_4/GCE. The biosensor was used successfully for selective and sensitive detection of glucose based on the decreasing of cathodic peak current of oxygen. The proposed biosensor applied for glucose determinations in human serum without any interference.

2. Experimental Section

2.1 Reagent and materials

Glucose oxidase (from Aspergillusniger, EC1.1.3.4.150,000 unit/g) and glucose (Sigma, 99%) were purchased from USA and used without further purification. p-Phenylenediamine,

ferric chloride ($FeCl_3 \cdot 6H_2O$), ferrous chloride ($FeCl_2 \cdot 4H_2O$), ammonium persulfate (APS), sodium dodecyl sulfate (SDS), and all solvents were purchased from Merck (Darmstadt, Germany) and were used without further purification. Phosphate buffer solutions (PBS) were prepared by mixing the stock solutions of 0.1 M NaH_2PO_4 and 0.1 M Na_2HPO_4, and then adjusting the pH with H_3PO_4 or NaOH. Fresh GOD (5 mg ml^{-1}) solutions were prepared in PBS and stored at 4 °C. The glucose stock solution was prepared by 0.1 M pH 7.0 PBS. All other chemicals were of analytical grade and were used as received without any purification process. All the supplementary chemicals were of analytical grades and solutions were prepared with 18.2 MΩ deionized water. The supporting electrolytes were used in all the experiments with 0.1 M PBS.

2.2 Apparatus

Autolab Electrochemistry Instruments (Autolab, Eco Chemie, Netherlands) were used for amperometry measurements. Cyclic voltammetry measurements were carried out on a Metrohm (797 VA Computrace, Switzerland) controlled by personal computer. A saturated calomel electrode (SCE) as reference electrode and a platinum wire as auxiliary electrode were used. A GCE, (Metrohm, Switzerland) with a geometrical area of 0.0314 cm^2, bare or modified, was used as working electrode. SEM, (Hitachi S4160 instrument) was used to obtain information on the morphology of nanocomposite. FT-IR spectra were recorded on a Bruker Tensor 27 spectrometer. A digital pH-meter (780 pH meter, Metrohm) with precision of ±0.001 was used to read the pH value of the buffer solutions. Electrolyte solutions were deoxygenated by purging pure nitrogen (99.99%) for 10 min prior to the electrochemical experiments. All measurements were carried out under a nitrogen atmosphere.

2.3 Preparation of Fe_3O_4 Nanoparticles

Fe_3O_4 NPs were synthesized according to previously reported chemical route [26,27]. Briefly, 1.07 g of $FeCl_2.4H_2O$ and 2.91 g of $FeCl_3.6H_2O$ were dissolved in 50 ml deionized water at room temperature. The mixture was stirred mechanically at 80 ℃ for 30 min under reflux condition and then (25%) NH_4OH (10 ml) was quickly added into the mixture until the pH reached 10. After 30 min, the black precipitate of Fe_3O_4 was separated by magnetic decantation and washed several times with deionized water and twice with ethanol. Finally, Fe_3O_4 NPs were dried at 80 ℃ under vacuum for 6 h. Fig. 1 shows the typical TEM image of the obtained Fe_3O_4 NPs with an average diameter of 30 nm.

Figure 1

2.4 Preparation of PPD@Fe_3O_4 nanocomposite

PPD@Fe_3O_4 nanocomposite was synthesized according to previously described procedure [20]. Typically, 0.75 g of Fe_3O_4 NPs, 2.65 g SDS and 20 ml chloroform were added into 30 ml of distilled water and the mixture dispersed by an ultrasonic bath at room temperature for 1 h. Then, 1 g p-phenylenediamine monomer in 30 ml HCl (1 M) solution was slowly added and the resulting solution continued to be stirred. The fresh APS solution (1.5 g of APS in 20 ml deionized water) was dropped into the reaction medium for 30 min. The reaction was carried out at room temperature for 24 h. Then the reaction mixture was poured into acetone to terminate the reaction. The formed precipitate was filtered and washed with distilled water for several times and methanol for once. Finally, the obtained red dark powder was dried in vacuum at 50℃ for 24 h. The prepared nanocomposites were stable at room temperature even after 6 months of storage.

2.5 Fabrication of the modified electrode

The GCE was carefully polished with alumina powder on polishing cloth and then sonicated in ethanol to remove adsorbed particles. Then 10 cycles scans were carried out in the potential window of –2.0 to +2.0 V vs. reference electrode in a solution of 1 M H_2SO_4, to remove impurities from the electrode surface. Finally, the GCE washed with deionized water and dried for 5 min at an oven. A 0.5 mg PPD@Fe_3O_4 nanocomposite was dispersed in 5 mL DMSO by ultrasonic agitation for about 5 min to give a suspension of 0.1 mg/mL. The resulting black nanocomposite suspension was spin-cast on the GCE at the speed of 500 rpm to make nanocomposite film. The prepared electrode named PPD@Fe_3O_4/GCE. The GOD-PPD@Fe_3O_4/GCE was obtained by casting the about 6 µl of GOD onto PPD@Fe_3O_4/GCE with spin-casting equipment at a speed of 400 rpm and allowed to dry at room temperature. The prepared electrodes were stored at 4 ◦C in a refrigerator when not in use. The total structure of the GOD-PPD@Fe_3O_4/GCE is showed in Scheme 1.

Scheme 1

3. Results and Discussion

3.1 Electrode characterizations

The FTIR spectra of native GOD, and GOD-PPD@Fe_3O_4 nanocomposite are presented in Fig. 2. In FTIR spectra of native GOD, the strong absorption at 3300 cm^{-1} is assigned to the N−H stretching, and the characteristic peaks were observed at 1650 and 1526 cm^{-1}, which are attributed to amide I (the C=O stretching vibrations of the peptide bond groups) and II (the N−H in-plane bending and C−N stretching modes of the polypeptide chains) bands of native GOD [28]. The FTIR spectrum of GOD-PPD@Fe_3O_4 also shows two characteristic adsorption bands at 1661 and 1526 cm^{-1}, proposing that GOD has been successfully immobilized on the PPD@Fe_3O_4 nanocomposite. The slight shift of the adsorption bands corresponding to amide I may come from intermolecular interaction between enzyme and

PPD@Fe_3O_4 nanocomposite, which can effectively increase the stability of GOD on the PPD@Fe_3O_4 matrix.

"Figure 2"

Characteristic SEM images of the PPD@Fe_3O_4/GCE and GOD-PPD@Fe_3O_4/GCE are shown in Fig. 3. Fig. 3a shows the three-dimensional netlike porous surface of PPD@Fe_3O_4/GCE. It is evident that Fe_3O_4 nanoparticles are distributed well in the PPD matrix and porous structure provided a large surface-to-volume ratio, which is able to make available large amounts of active GOD on the electrode. Fig. 3b shows immobilized GOD on the PPD@Fe_3O_4/GCE as a uniform surface. The three-dimensional structure of nanocomposite after immobilization of GOD is helpful for enhancing the DET of GOD.

"Figure 3"

3.2 Direct electrochemistry of GOD

Fig. 4 shows cyclic voltammograms of the GOD-GCE (curve a), GOD-PPD/GCE (curve b), GOD-PPD@Fe_3O_4/GCE (curve c) and PPD@Fe_3O_4/GCE (curve d) in N_2-saturated 0.1 M pH 7.0 PBS at scan rate of 100 mV s^{-1}. The cyclic voltammograms of both GOD-PPD/GCE and GOD-PPD@Fe_3O_4/GCE showed a pair of well-defined redox peaks. The formal redox potentials (defined as half of sum of anodic and cathodic peak potential, $E^{0'}$) are −0.49 V and −0.41 V (vs. SCE), respectively, which are close to the $E^{0'}$ value reported previously, attributed to the DET of GOD for the conversion of GOD(FAD) to GOD($FADH_2$) [29]. However, such redox process is unable to achieve at GOD-GCE under the same condition, suggesting that DET of GOD is not succeed at the surface of bare GCE. Moreover, no redox peaks observe at the PPD@Fe_3O_4/GCE. Hence, it can be concluded that PPD@Fe_3O_4 nanocomposite is operative to facilitate the DET between GOD and GCE. As it shown, in the

absence of Fe_3O_4 nanoparticles, the GOD-PPD/GCE (curve b) can also display a couple of redox peaks of GOD. However, the response is 2.3 times smaller than that of the GOD-PPD@Fe_3O_4/GCE, indicating that the presence of Fe_3O_4 nanoparticles in the nanocomposite plays an important role in facilitating the electron exchange between GOD(FAD)/GOD($FADH_2$) centers of GOD and the electrode surface. In fact, the presence of Fe_3O_4 nanoparticles improves the penetrability, morphology and conductivity of the nanocomposite and accelerates the electron transfer between GOD and the electrode surface.

"Figure 4"

Fig. 5A shows the voltammetric response GOD-PPD@Fe_3O_4/GCE in pH 7.0 at different scan rates ranging from 10 to 600 mV s^{-1}. Both the reduction and oxidation peak currents increase linearly relational to the scan rate in the range of 10–600 mVs^{-1}, indicating a surface controlled electrode process (Fig. 5B). It is clear that adsorbed GOD undertakes a reversible electron transfer onto the surface of modified electrode. The formal redox potential is almost independent of the potential scan rate for sweep rates below 140 mVs^{-1}. From the integration of the reduction peak of the GOD-PPD@Fe_3O_4/GCE at different scan rates, the average surface coverage (Γ) of GOD on the surface of modified GCE was calculated to be $(4.65\pm0.76)\times10^{-10}$ mol cm^{-2}. On the other hand, it was found that at scan rates of above 140 mVs^{-1}, ΔE_p increased with increasing scan rate. The values of both the anodic and cathodic potentials are proportional to the logarithm of the scan rate (Fig. 5C). The transfer coefficient (α) and apparent heterogeneous electron transfer rate constant (K_s) can be estimated by measuring the variation of peak potential with scan rate with Laviron theory according to the following equations [30]:

$$E_{pc}=E°'-(2.3RT/\alpha nF)\log \upsilon \quad (1)$$

$$E_{pa} = E°' + (2.3RT/(1 - \alpha)nF) \log \upsilon \quad (2)$$

$$\log k_s = \alpha \log(1-\alpha) + (1-\alpha)\log \alpha - \log (RT/nFv) - (1-\alpha)\, \alpha F\Delta E_p/2.3RT \quad (3)$$

where R is the gas constant, T is the room temperature and ΔE_p is the peak separation of the GOD(FAD)/GOD($FADH_2$) redox couple. According to Eqs. (1-3), the transfer coefficient and heterogeneous electron transfer rate constant were calculated 0.54 and 3.76 s^{-1}, respectively. The obtained k_s value was higher than that of GOD immobilized on functionalized carbon nanotubes (1.69 s^{-1}) [31], GOD incorporated in biomediated gold nanoparticles–carbon nanotubes composite film (2.2 s^{-1}) [19], graphene/chitosan (2.83 s^{-1}) [32], GOD immobilized onto graphene nanosheets and carbon nanospheres mixture (2.64 s^{-1}) [33], electrochemically reduced graphene oxide (ERGO)/poly l-lysine (3.27 s^{-1}) [34], GOD at poly(taurine) modified glassy carbon electrode (1.386 s^{-1}) [35], CNTs-poly(diallyldimethylammonium chloride) (PDDA) modified electrode (2.76 s^{-1}) [36] and GOD immobilized on graphene quantum dots modified carbon ceramic electrode (1.12 s^{-1}) [17]. This result suggested that comparing with other nanomaterial base or polymer composites; the porous PPD@Fe_3O_4 structure has more active sites on the surface, which cause to improve the communication between redox center of GOD and electrode.

"Figure 5"

The couple of FAD/$FADH_2$ at immobilized GOD on the surface of the PPD@Fe_3O_4 nanocomposite exhibit established and well defined redox peaks over the pH range of 4 to 9. From Fig. 6, the formal redox potential shifted positively with the decrease of pH, indicated the electrochemical manner accompanied protonated process more easily at low pHs. The plot of pH versus $E^{0'}$ (inset to Fig. 6) displays a linear dependence over the studied pH range. The slope value of -0.0614 VpH^{-1} is in close agreement with the obtained theoretical value of 0.0586 VpH^{-1} for a reversible redox process involving two electrons and two protons [37].

"Figure 6"

The stability is an important parameter for the evaluation of the biosensor performance. The stability of biosensor in absence and presence of Fe_3O_4 NPs, GOD-PPD/GCE and GOD-PPD@Fe_3O_4/GCE, was determined by measuring the response current of 100 μM glucose during a period of 30 days. When not in use, the biosensors were kept in a refrigerator at 4 °C. The results obtained for both biosensors were shown in Fig. 7, where i_0 is the response current of the biosensor freshly fabricated, i is the response current at any storage time, i-i_0 is the change in the response current at any storage time. GOD-PPD@Fe_3O_4/GCE exhibited good stability during 15 days and the response current remained about 95% of its initial response. After that, an activity loss of 12% was observed after 30 days. The lifetime of GOD-PPD/GCE was shorter than GOD-PPD@Fe_3O_4/GCE retained 85% of its initial response after 15 days. Such good stability of GOD-PPD@Fe_3O_4/GCE may be attributed to the presence of Fe_3O_4 NPs at nanocomposite. The reproducibility of GOD-PPD@Fe_3O_4/GCE towards glucose detection was also examined. The R.S.D. of inter-electrode responses to 100 μM glucose at five different electrodes was 6.22% while the R.S.D. of intra-electrode responses to five-times repeated additions of 100 μM glucose was 4.5%. These results show that the GOD-PPD@Fe_3O_4/GCE was very efficient for retaining high enzymatic activity and preventing enzyme leakage from the PPD@Fe_3O_4 nanocomposite, which was very important for the development of the proposed biosensor in low-cost application.

"Figure 7"

3.3 Performance of biosensor toward glucose determination

The influence of oxygen on application of biosensor was investigated in N_2-saturated (a and c), and O_2-saturated (b and d) PBS on the surface of PPD@Fe_3O_4/GCE (dash lines) and GOD-PPD@Fe_3O_4/GCE (solid lines) at scan rate 100 mV s^{-1} (Fig. 8A). A clear increase can be observed in reduction peak current and a simultaneous decrease in oxidation peak current

of GOD in the O_2-saturated PBS (curve b), demonstrating an electrocatalytic process toward reduction of dissolved oxygen occur at the GOD-PPD@Fe_3O_4/GCE [38]. Also, the electrocatalytic response of the biosensor towards glucose was compared under both N_2-saturated and O_2-saturated PBS solutions. Upon addition of glucose to O_2-saturated PBS, the reduction current response of biosensor decreased (Fig. 8B). The association between increase and decrease of cathodic current of biosensor in O_2-saturated PBS, at absence and presence of glucose, can be explained by following equations:

$$GOD(FAD) + 2H^+ + 2e^- \rightarrow GOD(FADH_2) \quad (4)$$

$$GOD(FADH_2) + O_2 \rightarrow GOD(FAD) + H_2O_2 \quad (5)$$

$$GOD(FAD) + glucose \rightarrow GOD(FADH_2) + gluconolactone \quad (6)$$

According to Eq. (5) and (6), GOD(FAD) groups can be produced from denatured GOD on the surface of electrode via catalysed reduction of oxygen. On the other hand, Eq. 6 shows the concentration of the oxidized form of GOD(FAD) on electrode surface decrease in the presence of glucose. Thus, the addition of glucose repressed the electrocatalytic reaction and led to the decrease in the reduction current.

"Figure 8"

3.4 Amperometric measurement of glucose at GOD-PPD@Fe_3O_4/GCE

In view of the excellent catalytic activity of GOD-PPD@Fe_3O_4/GCE towards the glucose sensing, amperometric detection of glucose is attempted. Fig. 9A shows the amperometric response of biosensor on successive injection of glucose into 0.1 M PBS buffer (pH 7.0) at an applied potential of -0.62 V with a time interval of ca. 20 s. Upon addition of glucose the reduction current decreased rapidly and could achieve 95% of the steady-state current within 4 s, indicating a fast amperometric response to glucose reduction. The response shows a

linear range from 5 to 1450 μM, with a correlation coefficient of 0.9934 and a slope of 0.0558±0.3 μA mM^{-1} (Fig. 9B). The limit of detection at a signal-to-noise ratio of 3 is estimated to be *ca.*1.9±0.06 μM, which is comparable with or, in most cases, lower than the reported value of 20 μM glucose oxidase GOD on three-dimensional interpenetrating, porous graphene modified electrode [39], 0.6 μM graphene/polyaniline/Au nanoparticles/glucose oxidase biocomposite [12], 60 μM GOD at poly(taurine) modified glassy carbon electrode [35], 2.8 μM GOD on a glass carbon electrode modified with MoS_2 nanosheets decorated with gold nanoparticles [40] and 0.06 mM GOD on polyaniline/poly(acrylic acid) composite film [41]. These results indicate that the fabricated biosensor has high bioelectrocatalytic activity toward glucose detection.

From the relationship between the reciprocal of current and the reciprocal of glucose concentration (Fig. 9C), the apparent Michaelis–Menten constant (K_m), an main parameter to expose enzyme-substrate reaction kinetics, is calculated to be 0.42 mM according to Lineweaver-Burk equation [20], which is much smaller than 9.85 mM of GOD in electropolymerized poly(o-phenylenediamine) film [42], 0.76 mM for GOD immobilized onto graphene quantum dots [17], 2.95 mM based on the immobilization of GOD onto a GCE grafted with 4-aminophenyl (AP) by diazonium chemistry [43]. The smaller K_m value suggests that the immobilized GOD hold enzymatic activity and exhibits notable attraction for glucose in the PPD@Fe_3O_4 nanocomposite.

"Figure 9"

3.5 Selectivity and real analysis applications

The selectivity of developed biosensor was investigated in solution of glucose after addition of possible interfering species such as of saccharose, galactose, fructose, ascorbic acid, uric acid, and dopamine. It was determined that these substrates have no effect on the analytical

signal. Similarly, interfering signals from some of cations and anions such as Ca^{2+}, Mg^{2+}, ClO_4^- and Cl^- do not influence the performance of the biosensor. The results are collected at Table 1. It suggests that biosensor is favorable for the selective determination of glucose in practical applications.

"Table 1"

With the purpose for the detection and recovery of glucose in real samples, GOD-PPD@Fe_3O_4/GCE was used for detection of glucose in human serum and urine samples. The samples obtained from a local laboratory under optimum conditions without any sample pretreatment other than a dilution step with PBS (pH 7.0) by the standard additional method. The determined results were compared with those obtained by a spectrophotometric method in a standard clinical laboratory. The detection results were presented in Table 2, which confirmed that the prepared GOD-PPD@Fe_3O_4/GCE can serve as an effective sensor for determination of glucose in real samples.

"Table 2"

4. Conclusions

In summary, a biosensor based on immobilization of GOD on PPD@Fe_3O_4 nanocomposite was fabricated for the determination of glucose. We have demonstrated PPD@Fe_3O_4 nanocomposite could provide a favorable microenvironment for immobilization of enzymes (here GOD) to retain their native structure and bioactivity. On the base of obtained results, PPD@Fe_3O_4 nanocomposite can act as a stable electron conducting bridge between the prosthetic groups of the GOD and the electrode surface and therefore can assist the direct electron transfer process. The GOD-PPD@Fe_3O_4 biosensor shows excellent electrocatalytic activity towards the determination of glucose together with worthy stability and repeatability.

Acknowledgement

We would like to thank the Hakim Sabzevari University for its financial support.

References

1 F. Y. Kong, S. X. Gu, W. W. Li, T. T. Chen, Q. Xu and W. Wang, *Biosens. Bioelectron.* 2014, **56**, 77–82.

2 J. D. Newman and A. P. F. Turner, *Biosens. Bioelectron*. 2005, **20**, 2435–2453.

3 S. Dönmez, F. Arslan, N. Sarı, N. Kurnaz Yetim and H. Arslan, *Biosens. Bioelectron.* 2013, **54**, 146–150.

4 A. Pandya, P. G. Sutariya and S. K. Menon, *Analyst* 2013, **138,** 2483–2490.

5 D. Zheng, S. K. Vashist, K. Al-Rubeaan, J. H. T. Luong and F. -S. Sheu, *Analyst* 2012, **137**, 3800–3805.

6 L. Meng, J. Jin, G. Yang, T. Lu, H. Zhang and C. Cai, *Anal. Chem.* 2009, **81**, 7271–7280.

7 Z. Yang, C. Zhang, J. Zhang and W. Bai, *Biosens. Bioelectron*. 2014, **51**, 268–273.

8 X. Zeng, X. Li, L. Xing, X. Liu, S. Luo, W. Wei, B. Kong and Y. Li, *Biosens. Bioelectron*. 2009, **24**, 2898–2903.

9 Y. Yu, Z. Chen, S. He, B. Zhang, X. Li and M. Yao, *Biosens. Bioelectron*. 2014, **52**, 147–152.

10 M. A. Kamyabi, N. Hajari, A. P. F. Turner and A. Tiwari, *Talanta* 2013, **116**, 801–808.

11 O. Yehezkeli, O. Ovits, R. Tel-vered, S. Raichlin and I. Willner, *Electroanalysis* 2010, **22**, 1817–1823.

12 Q. Xu, S. Gu, L. Jin, Y. Zhou and Z. Yang, *Sens. Actuators B: Chem*. 2014, **190**, 562–569.

13 Y. Zhang, W. Jia, M. Cui, C. Dong, S. Shuang, Y. K. Leung and M. M. F. Choi, *Biotechnol. J.* 2011, **6**, 492–500.

14 S. Palanisamy, C. Karuppiah and S. -M. Chen, *Colloids Surf., B* 2014, **114**, 164–169.

15 R. Cui, Z. Han, J. Pan, E. S. Abdel-Halim and J. -J. Zhu, *Electrochim. Acta* 2011, **58**, 179–183.

16 S. R. Nambiar, P. K. Aneesh and T. P. Rao, *Analyst* 2013, **138**, 5031–5038.

17 H. Razmi and R. Mohammad-Rezaei, *Biosens. Bioelectron*. 2013, **41**, 498–504.

18 K. -J. Huang, L. Wang, J. Li, T. Gan and Y. -M. Liu, *Measurement* 2013, **46**, 378–383.

19 H. Zhang, Z. Meng, Q. Wang and J. Zheng, *Sens. Actuators B: Chem*. 2011, **158**, 23–27.

20 M. Baghayeri, E. N. Zare and M. M. Lakouraj, *Biosens. Bioelectron*. 2014, **55**, 259–265.

21 X. Xiao, B. Zhou, L. Zhu, L. Xu, L. Tan, H. Tang, Y. Zhang, Q. Xie and S. Yao, *Sens. Actuators B: Chem*. 2012, **165**, 126–132.

22 M. Şenel and C. Nergiz, *Curr. Appl. Phys*. 2012, **12**, 1118–1124.

23 M. Baghayeri, E. N. Zare and R. Hasanzadeh, *Mater. Sci. Eng. C* 2014, **39**, 213–220.

24 M. Baghayeri, E. N. Zare and M. M. Lakouraj, *Sens. Actuators B: Chem*. 2014, **202**, 1200–1208.

25 M. Baghayeri, E. N. Zare and M. Namadchian, *Sens. Actuators B: Chem*. 2013, **188**, 227–234.

26 M. M. Lakouraj, E. N. Zare and P. N. Moghadam, *Adv. Polym. Tech*. 2014, **33**, 21385 (1-7)

27 E. N. Zare, M. M. Lakouraj and M. Baghayeri, *Int. J. Polym. Mater*. 2015, **64**, 175-183.

28 Z. Yang, X. Huang, R. Zhang, J. Li, Q. Xu and X. Hu, Electrochim. Acta 2012, **70**, 325–330.

29 P. Yang, L. Wang, Q. Wu, Z. Chen and X. Lin, *Sens. Actuators B: Chem*. 2014, **194**, 71–78.

30 E. Laviron, *J. Electroanal. Chem.* 1979, **101**, 19–28.

31 B. C. Janegitz, R. Pauliukaite, M. E. Ghica, C. M. A. Brett and O. Fatibello-Filho, *Sens. Actuators B: Chem*. 2011, **158**, 411–417.

32 X. Kang, J. Wang, H. Wu, I. A. Aksay, J. Liu and Y. Lin, *Biosens. Bioelectron*. 2009, **25**, 901–905.

33 H. Yin, Y. Zhou, X. Meng, K. Shang and S. Ai, *Biosens. Bioelectron*. 2011, **30**, 112–117.

34 L. Hua, X. Wu and R. Wang, *Analyst* 2012, **137**, 5716–5719.

35 R. Madhu, B. Devadas, S. M. Chen and M. Rajkumar, *Anal. Methods* 2014, **6**, 9053–9058.

36 Y. Yao and K. Shiu, *Electroanalysis* 2008, **20**, 1542–1548.

37 V. Mani, B. Devadas and S. -M. Chen, *Biosens. Bioelectron*. 2013, **41**, 309–315.

38 M. Baghayeri, H. Veisi, H. Veisi, B. Maleki and H. Karimi-Maleh, *RSC Advances* 2014, **4**, 49595–49604.

39 M. Cui, B. Xu, C. Hu, H. B. Shao and L. Qu, *Electrochim. Acta* 2013, **98**, 48–53.

40 S. Su, H. Sun, F. Xu, L. Yuwen, C. Fan and L. Wang, *Microchim. Acta* 2014, **181**, 1497–1503.

41 T. Homma, D. Sumita, M. Kondo, T. Kuwahara and M. Shimomura, *J. Electroanal. Chem.* 2014, **712**, 119–123.

42 E. Turkmen, S. Z. Bas, H. Gulce and S. Yildiz, *Electrochim. Acta* 2014, **123**, 93–102.

43 Z. Nasri and E. Shams, *Electrochim. Acta* 2013, **112**, 640–647.

Figure and scheme captions

Scheme 1. Schematic representation of fabrication of GOD-PPD@Fe_3O_4/GCE.

Fig. 1 The typical TEM image of the obtained Fe_3O_4 NPs.

Fig. 2 FTIR spectra of native GOD and GOD-PPD@Fe_3O_4 nanocomposite.

Fig. 3 SEM images of (a) PPD@Fe_3O_4/GCE and (b) GOD-PPD@Fe_3O_4/GCE.

Fig. 4 Cyclic voltammograms of the GOD-GCE (a), GOD-PPD/GCE (b), GOD-PPD@Fe_3O_4/GCE (c) and PPD@Fe_3O_4/GCE (d) in N_2-saturated 0.1 M pH 7.0 PBS at scan rate of 100 mV s^{-1}.

Fig. 5 (A) Cyclic voltammograms of GOD-PPD@Fe_3O_4/GCE in 0.1 M PBS (pH 7.0) at different scan rates of (1) 10, (2) 20, (3) 40, (4) 60, (5) 80, (6) 100, (7) 140, (8) 180, (9) 200, (10) 250, (11) 300, (12) 400, (13) 500 and (14) 600 mV s^{-1}. (B) Plot of the anodic (a) and cathodic (c) peak current against the scan rate. (C) Relationship of the anodic (a) and cathodic (c) peak potential against log υ.

Fig. 6 Cyclic voltammograms of the GOD-PPD@Fe_3O_4/GCE in 0.1 M PBS at different pHs. Scan rate: 100 mV s^{-1}. pH (from 5.0 to 9.0): 6.0, 7.0, 8.0, 9.0. Inset: plots of formal potential vs. pH.

Fig. 7 Stability of GOD-PPD/GCE and GOD-PPD@Fe_3O_4/GCE. Each data point of graph is based on measuring the amperometric response of 100 μM glucose in 0.1 M, pH 7.0 PBS at the applied potential of 0.62 V.

Fig. 8 (A) Cyclic voltammograms of GOD-PPD@Fe_3O_4/GCE in N_2-saturated (a) and O_2-saturated (b) 0.1 M, pH 7.0 PBS at 100 mV s^{-1}. (B) Cyclic voltammograms of GOD-

PPD@Fe_3O_4/GCE in N_2-saturated (c) and O_2-saturated 0.1 M, pH 7.0 PBS containing 0, 0.1, 0.3, 0.5, 0.7 and 0.9 mM glucose (from (i) to (d)) at scan rate of 100 mV s^{-1}.

Fig. 9 (A) Amperometric response of the biosensor to successive addition of different concentration of glucose into a stirring O_2-saturated 0.1 M PBS (pH 7.0) at the working potential of -0.62 V. (B) Plot of electrocatalytic peak current versus concentration of glucose. (C) Plot of the reciprocal of steady-state current (I_{ss}) versus the reciprocal of glucose concentration for the GOD-PPD@Fe_3O_4/GCE.

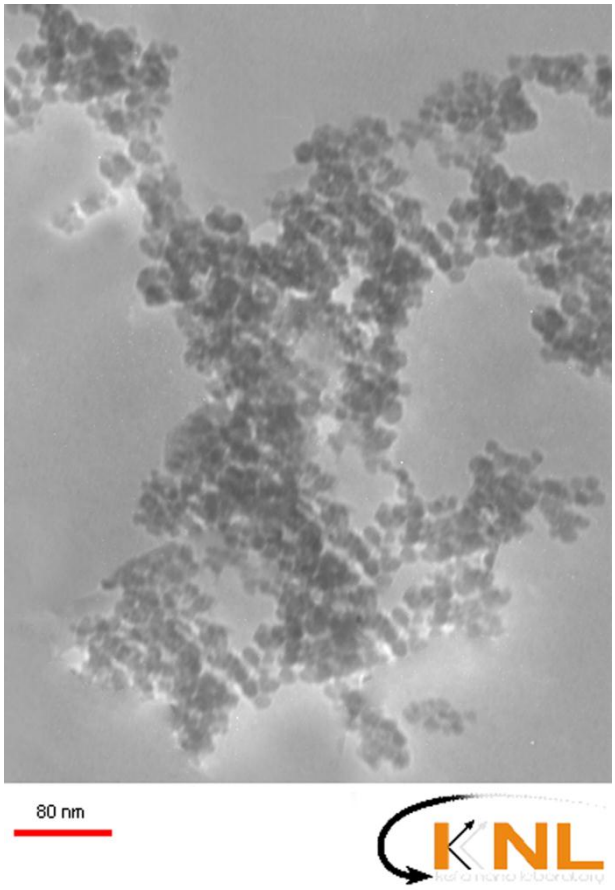

Figure 1

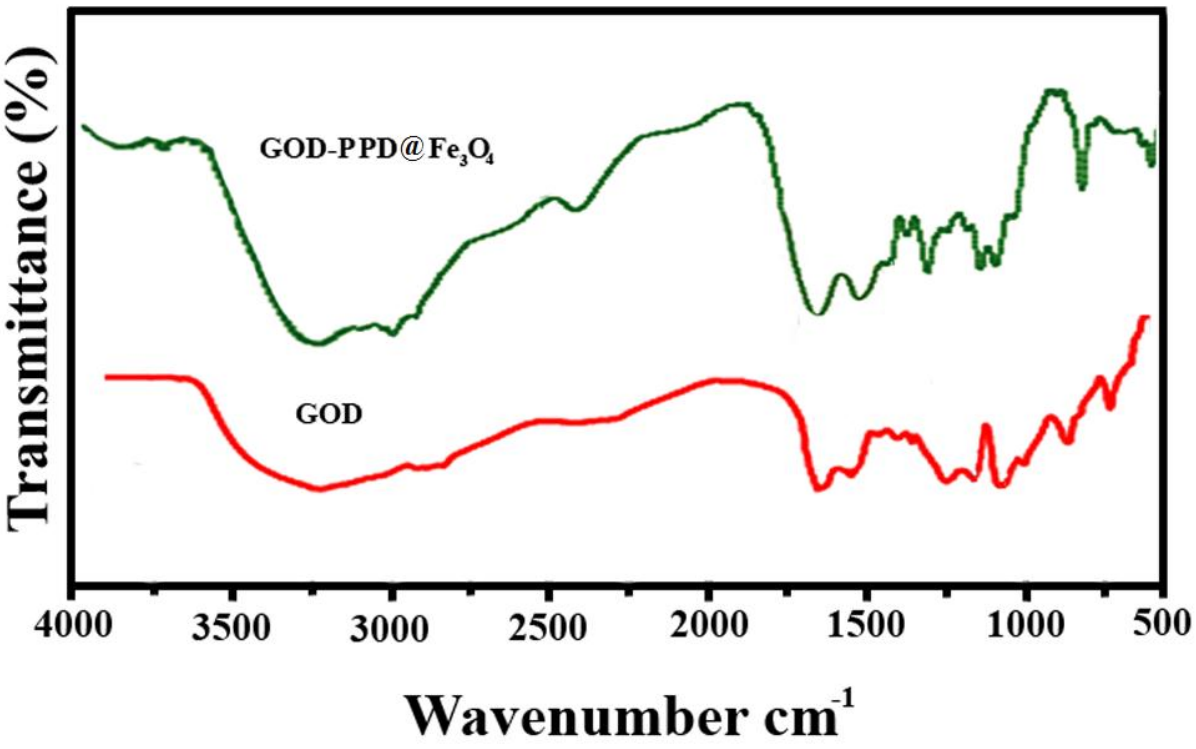

Figure 2

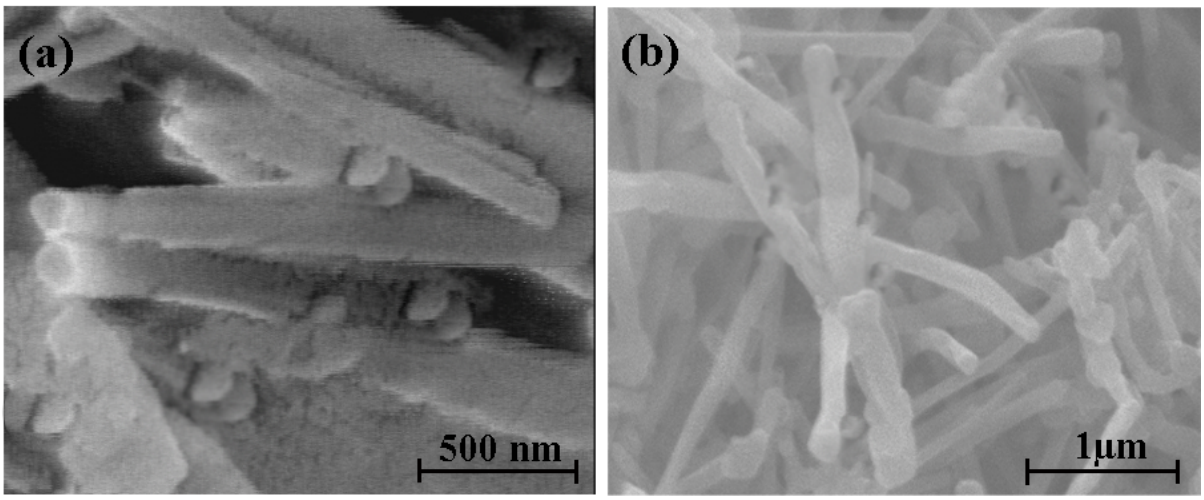

Figure 3

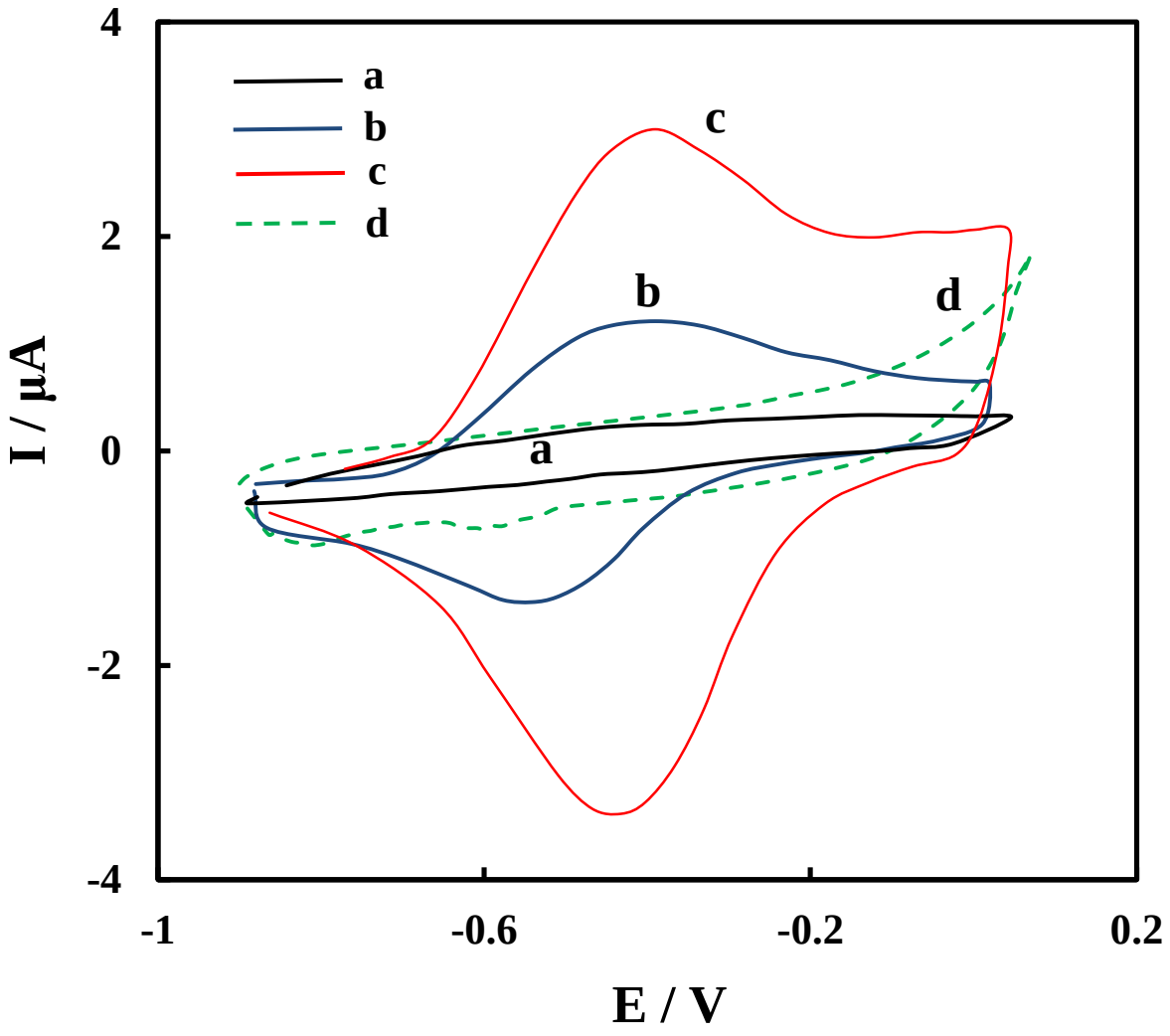

Figure 4

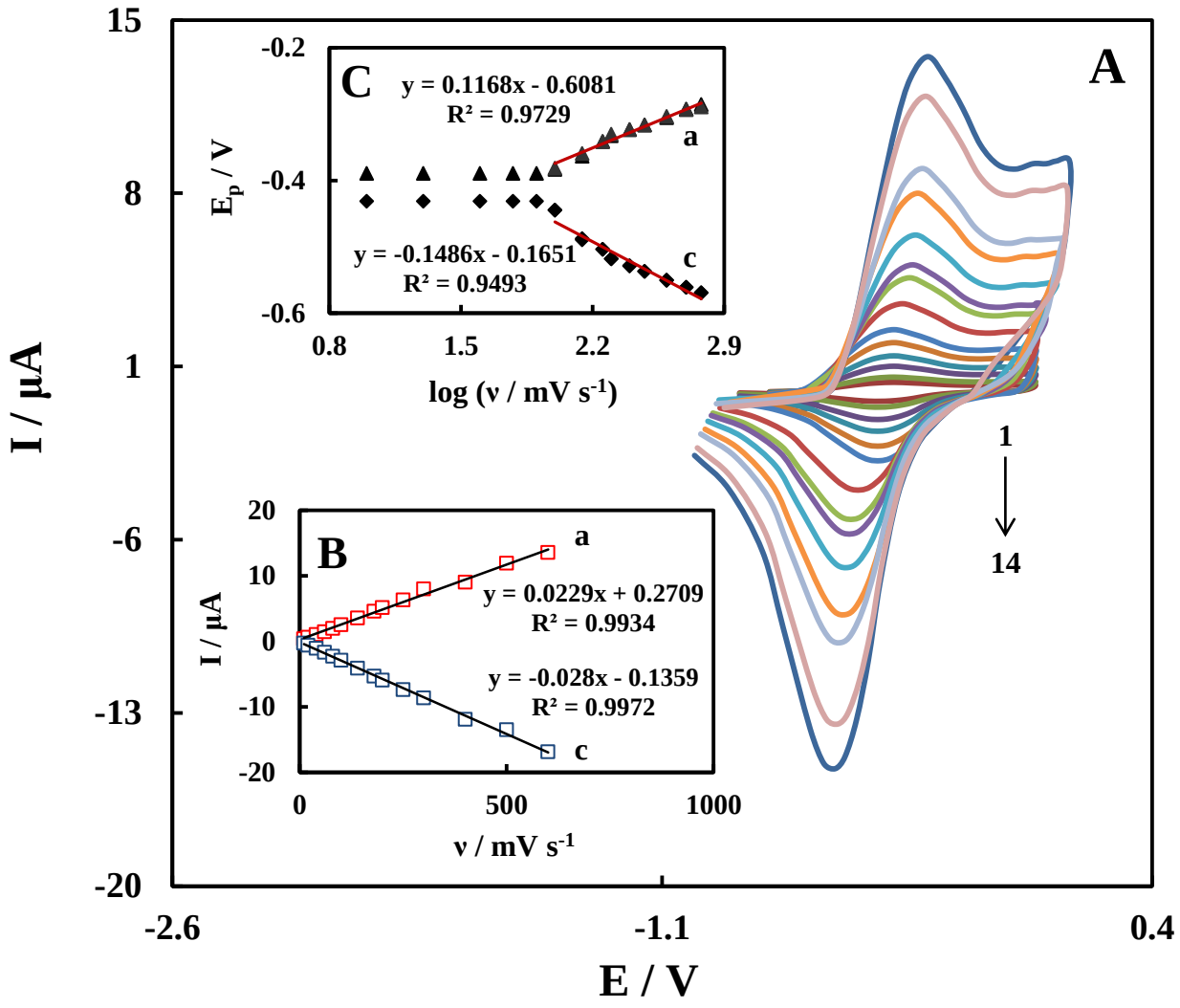

Figure 5

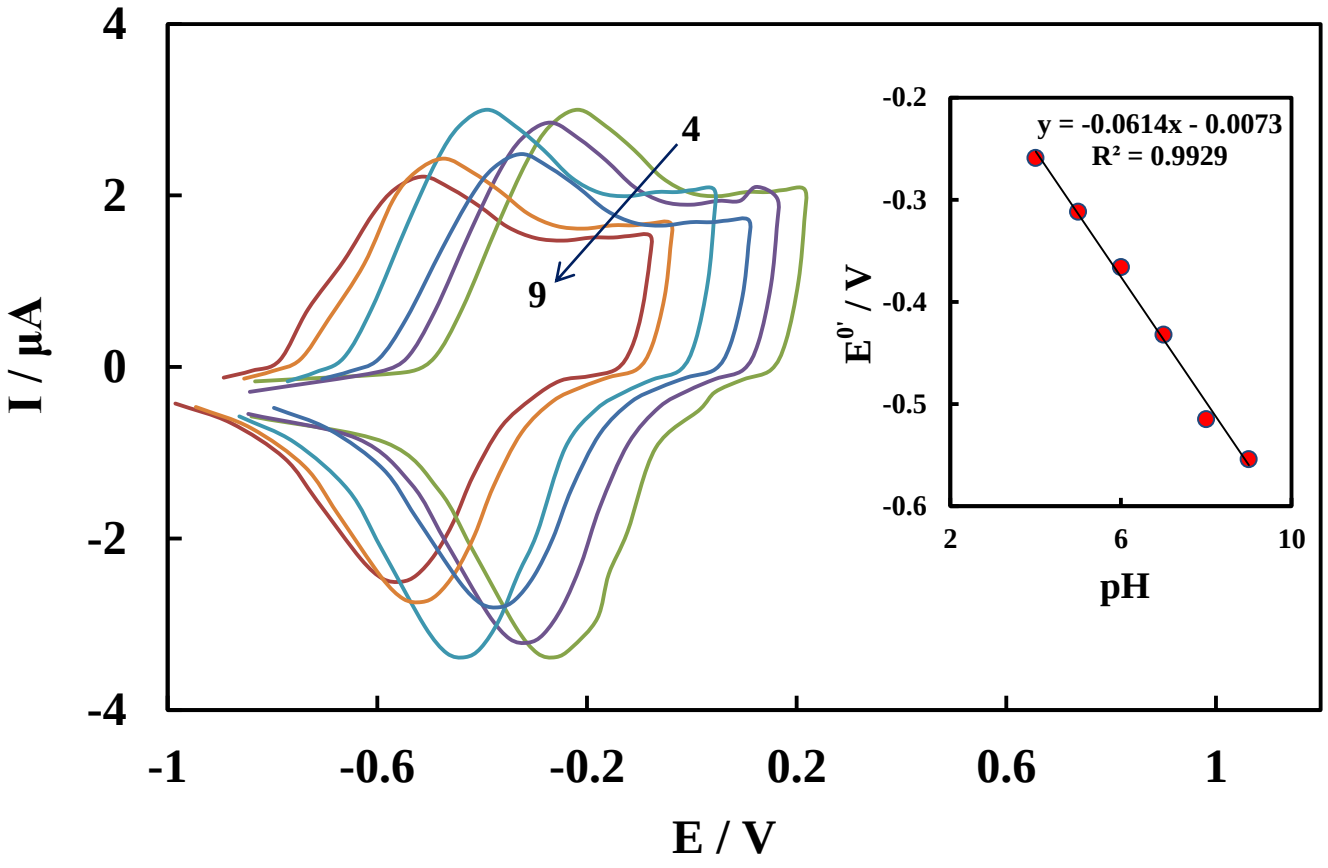

Figure 6

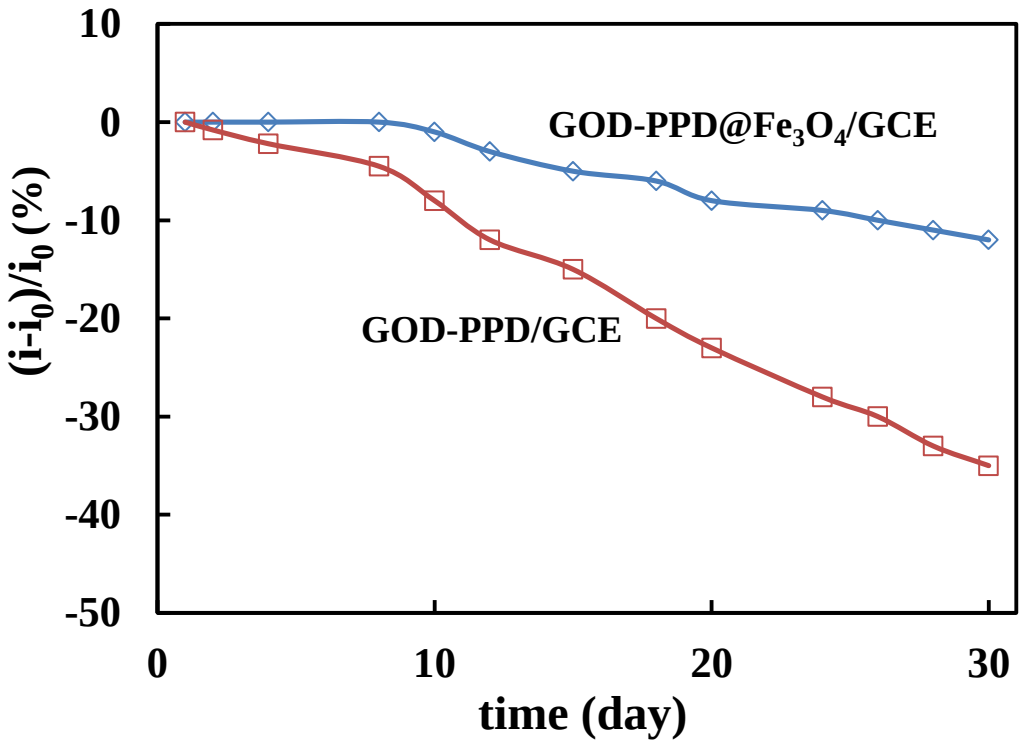

Figure 7

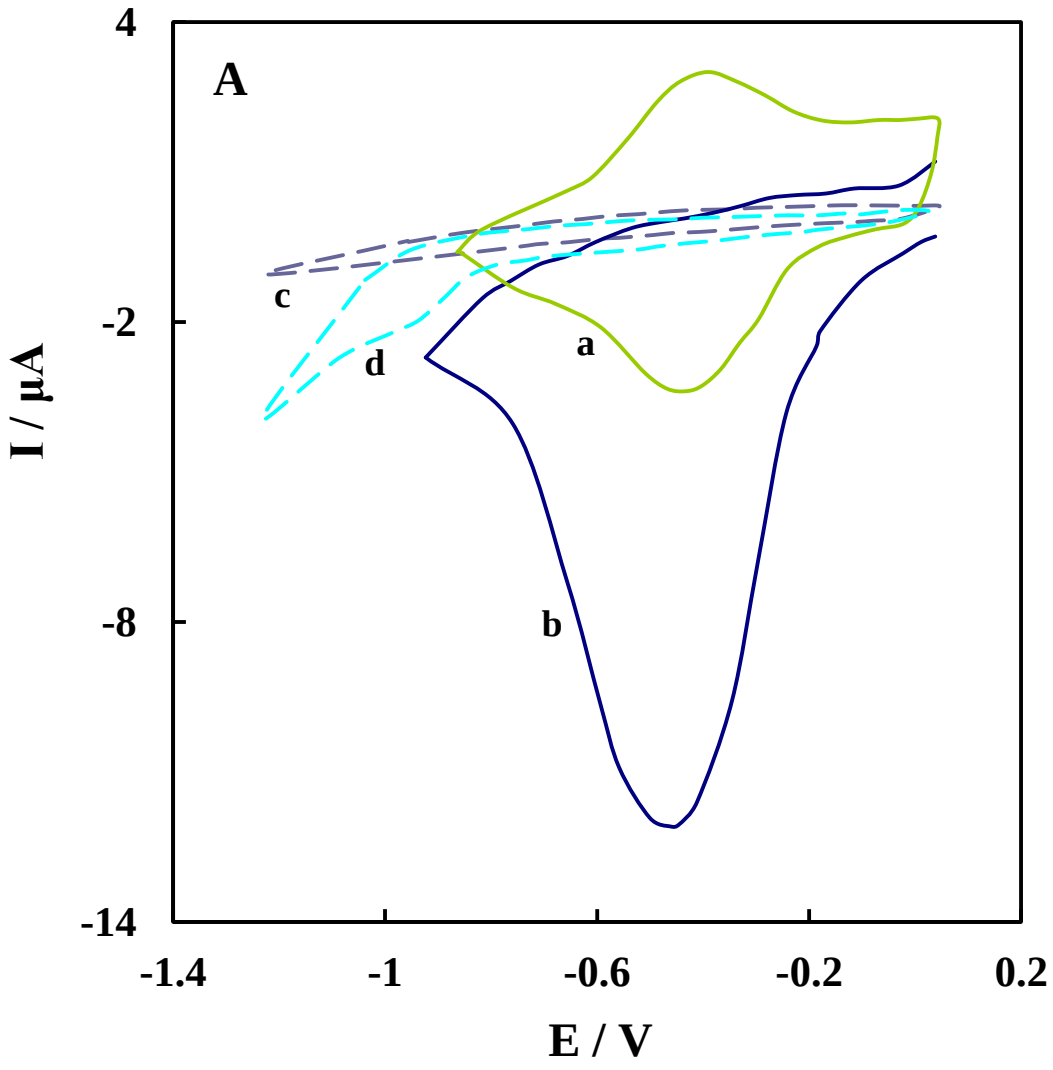

Figure 8A

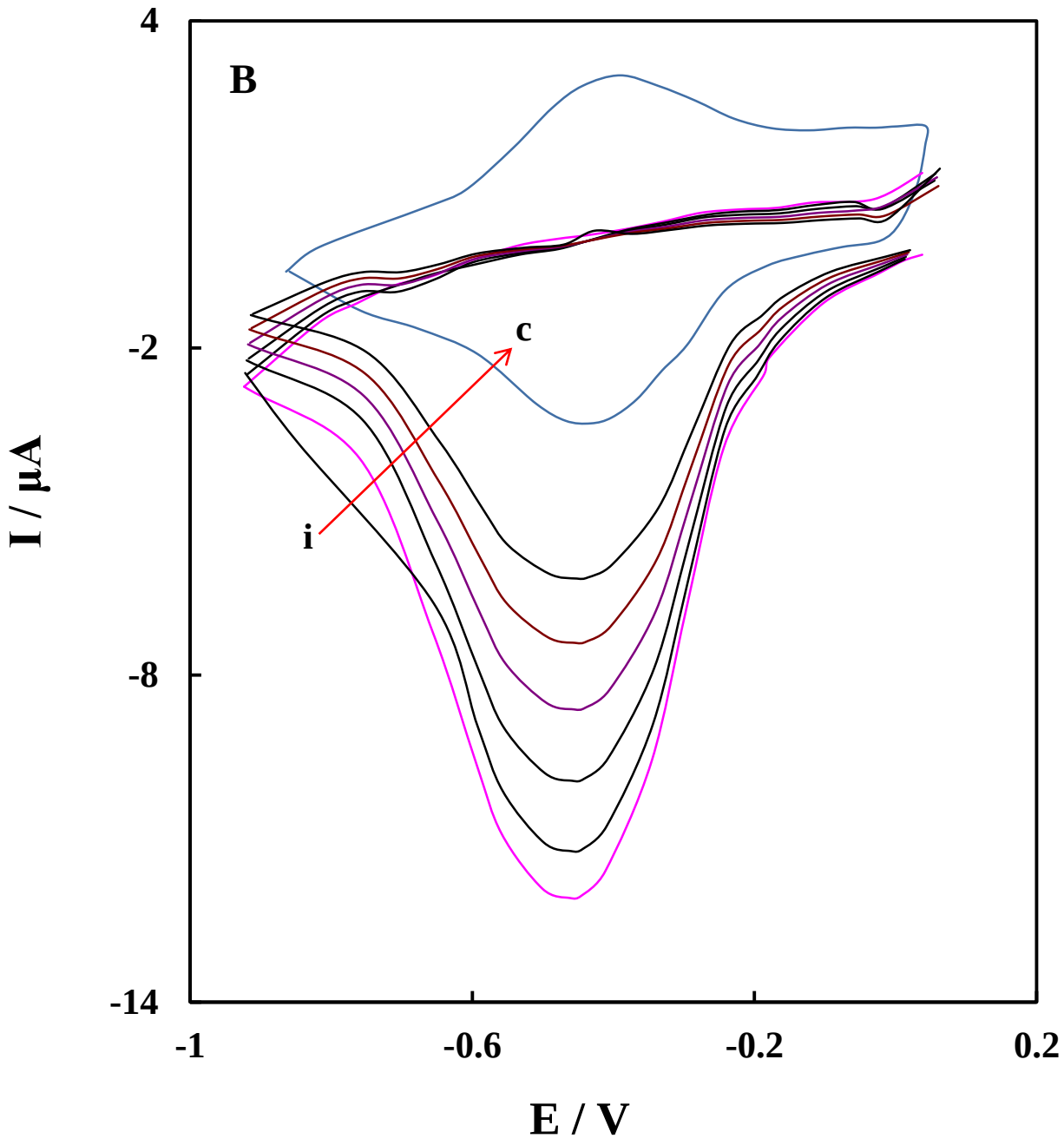

Figure 8B

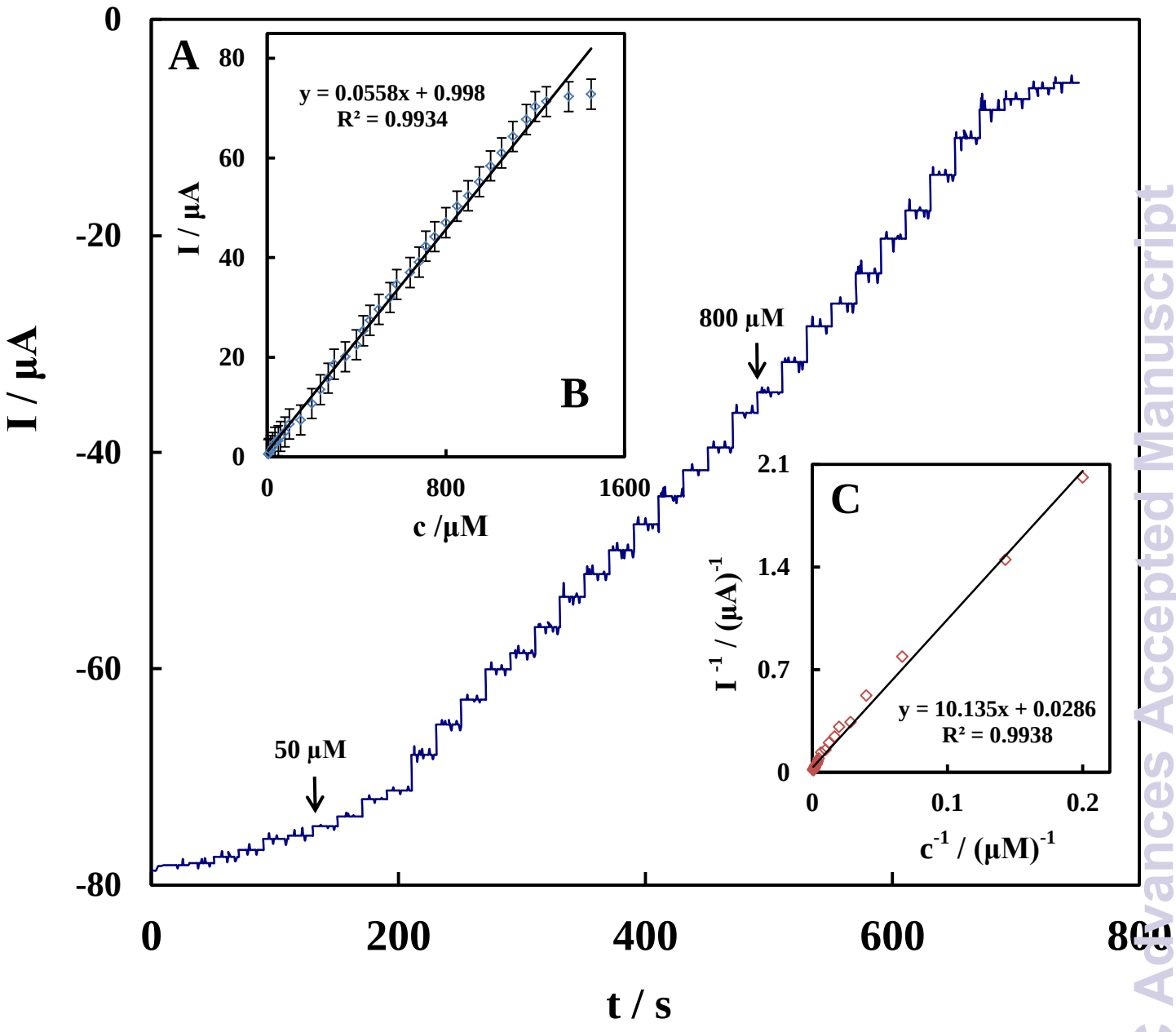

Figure 9

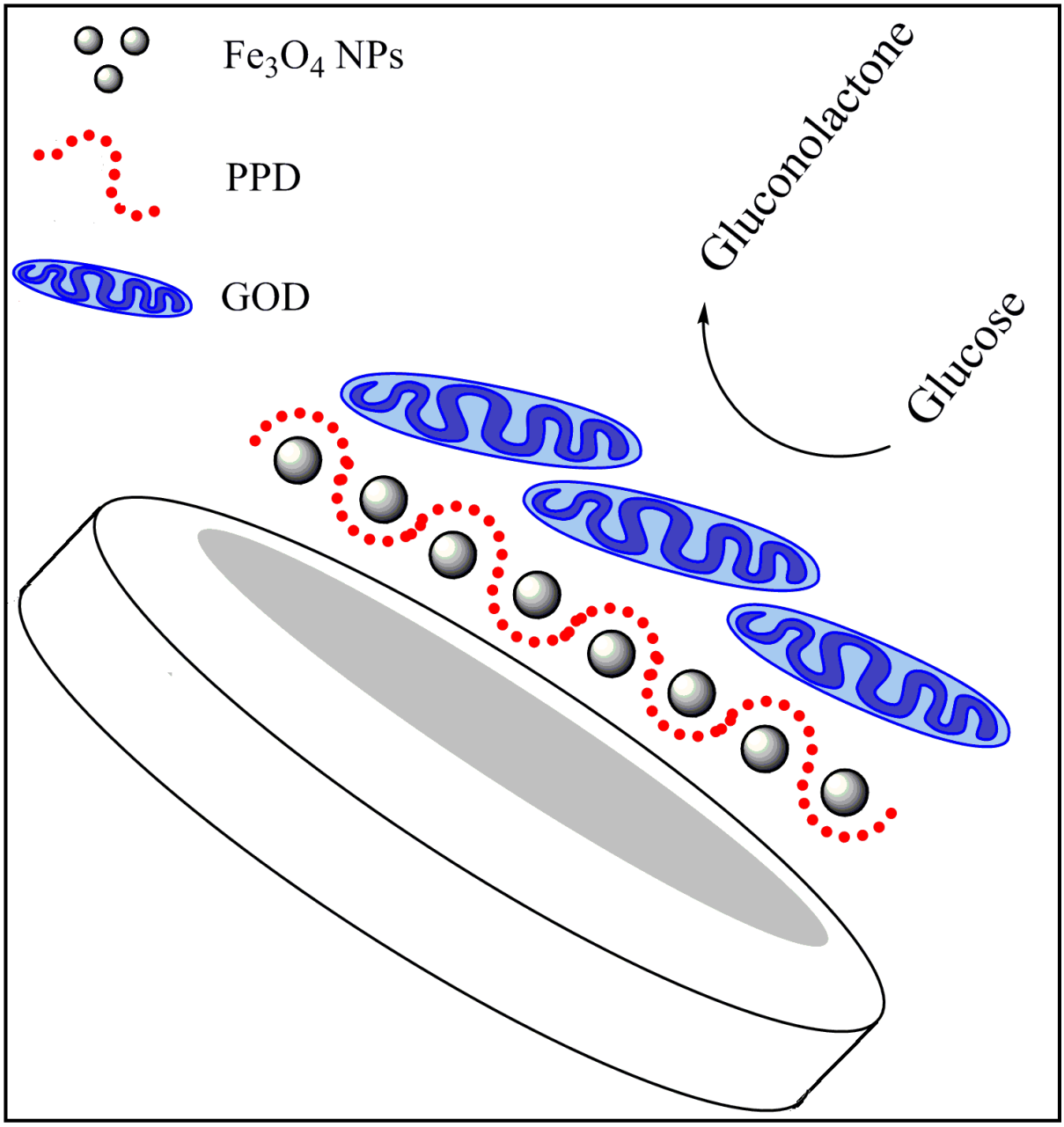

Scheme 1

Table 1

Investigation of some interfering agents on the glucose determination at fabricated biosensor.

Substrates [a]	Response current[b] (μA)	Current ratio[c]
Glucose	35.5± 0.06	-
Glucose + saccharose	35.8± 0.05	1.00
Glucose + galactose	36.0± 0.03	1.01
Glucose + fructose	35.4± 0.06	99.7
Glucose + ascorbic acid	35.4± 0.04	99.7
Glucose + uric acid	35.4± 0.04	99.7
Glucose + dopamine	35.4± 0.04	99.7
Ions effect		
Glucose + Ca^{2+}	35.5± 0.06	1.00
Glucose + Mg^{2+}	35.5± 0.06	1.00
Glucose + ClO_4^-	35.5± 0.06	1.00
Glucose + Cl^-	35.5± 0.06	1.00

[a]The concentrations of substrates were glucose: 1.0 mM; saccharose: 2.0 mM, galactose: 3.0 mM, fructose: 2.0 mM, ascorbic acid: 1.0 mM, uric acid: 1.0 mM, dopamine: 1.0 mM, Ca^{2+}: 1.0 mM, Mg^{2+}: 1.0 mM, ClO_4^-: 1.0 mM and Cl^-: 1.0 mM.

[b]Average of five determinations ± standard deviation.

[c]Current ratio is the current from a mixture of interfering substances and glucose (with mentioned concentrations) vs. the current from 1.0 mM glucose alone. Assay solution: 0.1 M pH 7.0 PBS.

Table 2

Results of the glucose detection and the recovery test for real sample analysis (n=5).

Serum sample	Added (mM)	Found (mM)	Determined by spectrophotometry	Recovery (%)
A	0	0.64±0.07	0.67	-
	0.3	0.96±0.06		102.1
	0.5	1.13±0.03		99.12
B	0	0.78±0.05	0.76	-
	0.2	0.97±0.05		98.97
	0.6	1.40±0.04		101.4
C	0	-	-	-
	0.2	0.193±0.05	0.21	96.5
	0.4	0.41±0.04	0.41	102.5
D	0	-	-	-
	0.3	0.306±0.04	0.295	102
	0.5	0.507±0.07	0.51	101.4

A and B samples of glucose in human serum.

C and D samples of glucose in human urine.